In Silico Radiation Oncology: Combining Novel Simulation Algorithms With Current Visualization Techniques

GEORGIOS S. STAMATAKOS, DIMITRA D. DIONYSIOU, EVANGELIA I. ZACHARAKI,
NIKOLAOS A. MOURAVLIANSKY, STUDENT MEMBER IEEE,
KONSTANTINA S. NIKITA, SENIOR MEMBER, IEEE, AND
NIKOLAOS K. UZUNOGLU, SENIOR MEMBER, IEEE

Invited Paper

The concept of in silico radiation oncology is clarified in this paper. A brief literature review points out the principal domains in which experimental, mathematical, and three-dimensional (3-D) computer simulation models of tumor growth and response to radiation therapy have been developed. Two paradigms of 3-D simulation models developed by our research group are concisely presented. The first one refers to the in vitro development and radiation response of a tumor spheroid whereas the second one refers to the fractionated radiation response of a clinical tumor in vivo based on the patient's imaging data. In each case, a description of the salient points of the corresponding algorithms and the visualization techniques used takes place. Specific applications of the models to experimental and clinical cases are described and the behavior of the models is two- and three-dimensionally visualized by using virtual reality techniques. Good qualitative agreement with experimental and clinical observations strengthens the applicability of the models to real situations. A protocol for further testing and adaptation is outlined. Therefore, an advanced integrated patient specific decision support and spatio–temporal treatment planning system is expected to emerge after the completion of the necessary experimental tests and clinical evaluation.

Keywords—Cancer, fractionation, in silico radiation oncology, modeling, Monte Carlo, radiation therapy, simulation, tumor growth, visualization.

I. INTRODUCTION

Cancer [1, pp. 1247–1294], [2, pp. 1006–1096], [3]–[5] is the second most frequent cause of death in the developed countries. Approximately 60% of all cancer patients in Europe and the United States receive radiation therapy (external beam therapy, brachytherapy) each year as therapy, or for palliation, or as an adjunct to surgery or chemotherapy. In order to achieve the best outcome for the patient in terms of tumor control and complication frequency, an optimization process of the treatment planning should take place before the radiation delivery.

Current treatment planning algorithms are based on the concept of physical optimization of the dose distribution and rely on rather crude biological models of tumor and normal tissue response. Such algorithms practically ignore the highly complicated dynamic behavior of malignant cells and tissues. The introduction of advanced biosimulation methods based on cell proliferation mechanisms and also on information drawn from the cellular and molecular properties of each individual malignancy and each individual patient are expected to substantially improve the radiation therapy efficiency. This would be accomplished by using alternative fractionations, spatial dose distributions, and even combination with other therapeutic modalities such as chemotherapy or hyperthermia.

Therefore, efficient modeling, simulation, and visualization of the biological phenomena taking place before, during, and after irradiation is of paramount importance. It is pointed out that the extremely high degree of complexity characterizing the corresponding elementary biological phenomena and their interactions makes it very difficult or even impossible to reliably describe tumor growth and response to irradiation by using simple analytical models. On the contrary, discrete time algorithmic descriptions (simulations) of the various phenomena offer the possibility of taking into account a large number of involved mechanisms and interactions.

The same philosophy has already been extensively applied to purely technological problems, and the emerged numerical methods [e.g., the finite difference time domain (FDTD) technique] have proved to be very efficient and reliable. A further prominent characteristic of the biological phenomena under consideration is stochasticity. For example, the fate of a single irradiated cell cannot be accurately predicted. Only survival probabilities can be assigned to the cell based on the accumulated experimental and clinical observations made on large cell populations. Furthermore, the exact spatio–temporal distribution of the various cell cycle phases within the tumor volume is generally unknown, although some plausible macroscopic hypotheses can be made. Therefore, stochastic techniques such as the generic Monte Carlo method seem to be particularly appropriate to the prediction of tumor growth and response to radiation therapy.

The practical usefulness of such methods is both to improve understanding of the cancer behavior and to optimize the spatio–temporal treatment plan by performing *in silico* (=on the computer) experiments before the actual delivery of radiation to the patient. In other words, the clinician could perform computer simulations of the likely tumor and adjacent normal tissue response to different irradiation scenarios based on the patient's individual imaging, histologic, and genetic data. The simulation predictions would support him or her in selecting the most appropriate fighting strategy. To this end, a substantial number of experimental and mathematical models have been developed. On the contrary, a rather small number of actual three-dimensional (3-D) computer simulation models have appeared in the literature. Exploitation of the potential of current visualization techniques is even more limited.

The aim of the present paper is to describe novel Monte Carlo simulation algorithms of tumor growth and response to irradiation, specific applications of the algorithms and 3-D visualization of the predicted outcome. The paper begins with a brief literature review concerning experimental, mathematical, and computer simulation models of tumor growth, angiogenesis, and tumor and normal tissue response to radiation therapy. Reference to papers describing visualization algorithms used in oncologic simulations is also made. As examples of radio-oncologic simulations, both an *in vitro* and an *in vivo* computer simulation model of tumor growth and response to radiation therapy are presented. An outline of the algorithms concerning cell division and interaction, cell response to irradiation, tumor expansion and shrinkage, as well as the procedures of data acquisition and visualization is given. Specific applications of the proposed models to the case of grade IV astrocytoma clarify the behavior of the simulation procedure. The paper concludes with a critical evaluation of the presented paradigms and suggestions on further research.

II. BRIEF LITERATURE REVIEW

In the past four decades, intensive efforts have been made in order to model tumor growth and tumor and normal tissue response to various therapeutic schemes such as radiation

therapy. As the corresponding literature is particularly extended, only indicative examples of the modeling efforts are given in the following paragraphs.

Experimental models of tumor growth include two-dimensional (2-D) and 3-D cell cultures (*in vitro* experimentation) and induction of tumors in laboratory animals (*in vivo* experimentation) [6]–[11]. Mathematical models of tumor growth attempt to analytically describe various aspects of the highly complex process such as diffusion of oxygen and glucose [12], [13], control stability [14], competition between tumor and host [15], interdependence between structure and growth [16] and growth and stability [17], [18], temporal profile of tumor cell proliferation [19]–[21], tumor cell replication rules [22], [23], invasion [24], metastasis [25], cell-cycle checkpoints [26], and angiogenesis [27]–[29]. The following approaches constitute representative examples of the modeling efforts. Adam and Maggelakis [12] analytically modeled the overall growth of a tumor spheroid using information about inhibitor production rates, oxygen consumption rates, volume loss and cell proliferation rates, and measures of the degree of nonuniformity of the various diffusion processes that take place. Casciari *et al.* [13] developed empirical correlations from experimental data to express EMT6/Ro tumor cell growth rates, oxygen consumption rates, and glucose consumption rates as functions of oxygen concentration, glucose concentration, and extracellular pH. Duechting [14] proposed a block diagram describing the growth of normal cells as well as the growth of benign and malignant tumors. He studied frequency and transition responses, locus diagrams, and stability conditions. Gatenby [15] developed a population ecology mathematical model examining tumors as part of a dynamic society of interacting malignant and normal cells. Rizwan-Uddin and Saeed [16] presented predictions of a mathematical model of mass transfer in the development of a tumor, resulting in its eventual encapsulation and lobulation. Michelson and Leith [29] modeled the effect of the angiogenic signals of basic fibroblast growth factor (bFGF) and vascular endothelial growth factor (VEGF) on the adaptive tumor behavior.

Computer simulation models aim at three-dimensionally reconstructing a growing tumor based on the behavior of its constituent parts (either single cells or clusters of cells). Such models have been used in order to study, e.g., the emergence of a spheroidal tumor in nutrient medium [30]–[38], the growth and behavior of a tumor *in vivo* [39]–[42], and the neovascularization (angiogenesis) process [31]. Duechting [31] developed a 3-D simulation model of tumor growth *in vitro* by combining systems analysis, control theory, and cellular automata. Wasserman and Acharya [39] developed a macroscopic tumor growth model mainly based on the mechanical properties of the tumor and the surrounding tissues. Kansal *et al.* [40], [41] proposed a 3-D cellular automaton model of brain tumor growth by using four parameters and introducing an adaptive grid lattice.

Experimental models of tumor response to radiation therapy primarily aim at determining the survival probability of the irradiated cells as a function of the absorbed

dose (survival curves). The values of many other parameters of interest can also be estimated [43]–[45]. Mathematical models attempt to analytically describe the effect of ionizing radiation to tumor and normal tissue cells [5], [46]–[63]. Thames *et al.* [46] mathematically described the dissociation between acute and late radiation responses with changes in dose per fraction. Dale [51] extended the classical linear quadratic dose–effect relationship in order to examine the consequences of performing fractionated treatments for which there is insufficient time between fractions to allow complete damage repair. Fowler [53] reviewed the considerable progress achieved in fractionated radiotherapy due to the use of the linear quadratic model. Zaider and Minerbo [60] proposed a mathematical model of the progression of cells through the mitotic cycle under continuous low-dose-rate irradiation and applied it to studies of the effects of dose rate on HeLa cells. Jones and Dale [62] presented various modifications of the linear quadratic model that were used in order to optimize dose per fraction. Of special importance are the recent attempts to mathematically model the effect of specific genes (e.g., the p53 status) to the radiation response of tumors [64]. Haas-Kogan *et al.* [64] modeled two distinct cellular responses to irradiation, p53-independent apoptosis and p53-dependent G_1 arrest that characterize the radiation response of glioblastoma cells using the linear quadratic model. Mathematical modeling of chemotherapy and other treatment modalities that may be applied in parallel with radiation therapy has also been developed [65], [66].

Computer simulation models aim at three-dimensionally predicting and visualizing the response of a tumor [67]–[76], [36] or normal tissue [70] to various schemes of radiation therapy as a function of time. Nahum and Sanchez-Nieto [68] presented a computer model based on the concept of the tumor control probability (TCP) and studied TCP as a function of the spatial dose distribution. Stamatakos *et al.* [71] developed a 3-D discrete radiation response model of an *in vitro* tumor spheroid and introduced high-performance computing and virtual reality techniques in order to visualize both the external surface and the internal structure of a dynamic tumor. Kocher *et al.* [75] developed a simulation model of tumor response to radiosurgery (single-dose application) and studied the vascular effects.

Finally, extensive work is being done on the combination of advanced visualization techniques, high-performance computing, and the World Wide Web capabilities in order to integrate and clinically apply the oncological simulation models [32]–[37], [77]–[79].

III. *In Vitro* Tumor Growth and Response to Radiation Therapy: An *in Silico* Model

The assumptions and the Monte Carlo treatment that follow pertain to the *in vitro* simulation model developed by our research group [32]–[37], [71], [72]. The modeling approach of Duechting [14], [30], [69], [80] has been adopted and substantially extended.
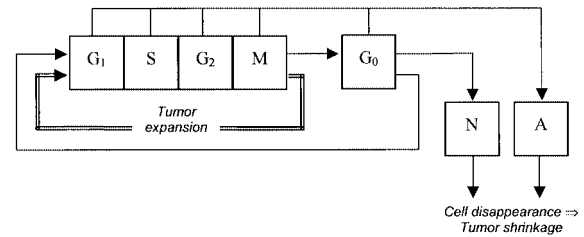
Fig. 1. Cytokinetic model of a tumor cell. Symbol explanation: G_1: G_1 phase; S: DNA synthesis phase; G_2: G_2 phase; G_0: G_0 phase; N: necrosis; A: apoptosis.

A. Cell Division and Interaction

The following fundamental assumptions have been made.

1) The cytokinetic model shown in Fig. 1 is adopted. According to this model, a tumor cell when cycling passes through the phases G_1 (gap 1), S (DNA synthesis), G_2 (gap 2), and M (mitosis) [1]–[4]. After mitosis is completed, each one of the resultant cells re-enters G_1 if the oxygen and nutrient supply in its current position is adequate. Otherwise, it enters the resting G_0 phase. It can stay there for a limited time T_{G0} if the oxygen and nutrient supply are inadequate. Subsequently, it enters the necrotic phase leading to cell death unless the local environment of the cell becomes adequate before the expiration of T_{G0}. In the latter case, the cell re-enters G_1.

2) In addition to the previously described pathway, there is always a probability that each cell residing in any phase (other than necrosis or apoptosis) dies with some probability per hour due to both ageing and spontaneous apoptosis. This probability representing the cell loss rate due to apoptosis is the product of the cell loss factor due to apoptosis (e.g., 10%) and the cell birth rate [3, p. 15]. The cell birth rate can be considered as the ratio of the growth fraction (e.g., 40%) [3, p. 15] to the cell cycle duration.

3) Angiogenesis is not taken into account. This is a plausible hypothesis for both tumor growth in cell culture (where there is no possibility for blood vessel formation) and the avascular early stages of tumor growth *in vivo*.

4) Side effects, immunologic reactions, heterogeneity, and the formation of metastases are neglected.

5) The following heuristic rules governing cell reproduction and interaction are applied: "if the minimum distance between a proliferating (cycling) tumor cell and the nutrient medium becomes greater than three cell layers, the tumor cell enters the G_0 phase." Inversely, "if the minimum distance between a tumor cell residing at the G_0 phase and the nutrient medium becomes less than three cell layers, the tumor cell reenters the cell cycle." These rules constitute a rough description of the oxygen and glucose diffusion dependent phenomena.

B. Tumor Cell Response to Irradiation

1) Cells in any cell cycle phase are more radiosensitive than hypoxic cells residing in G_0. Cells in the S phase are more radioresistant than cells in any other cycle phase (G_1, G_2, and M). Three different sets of values for the α
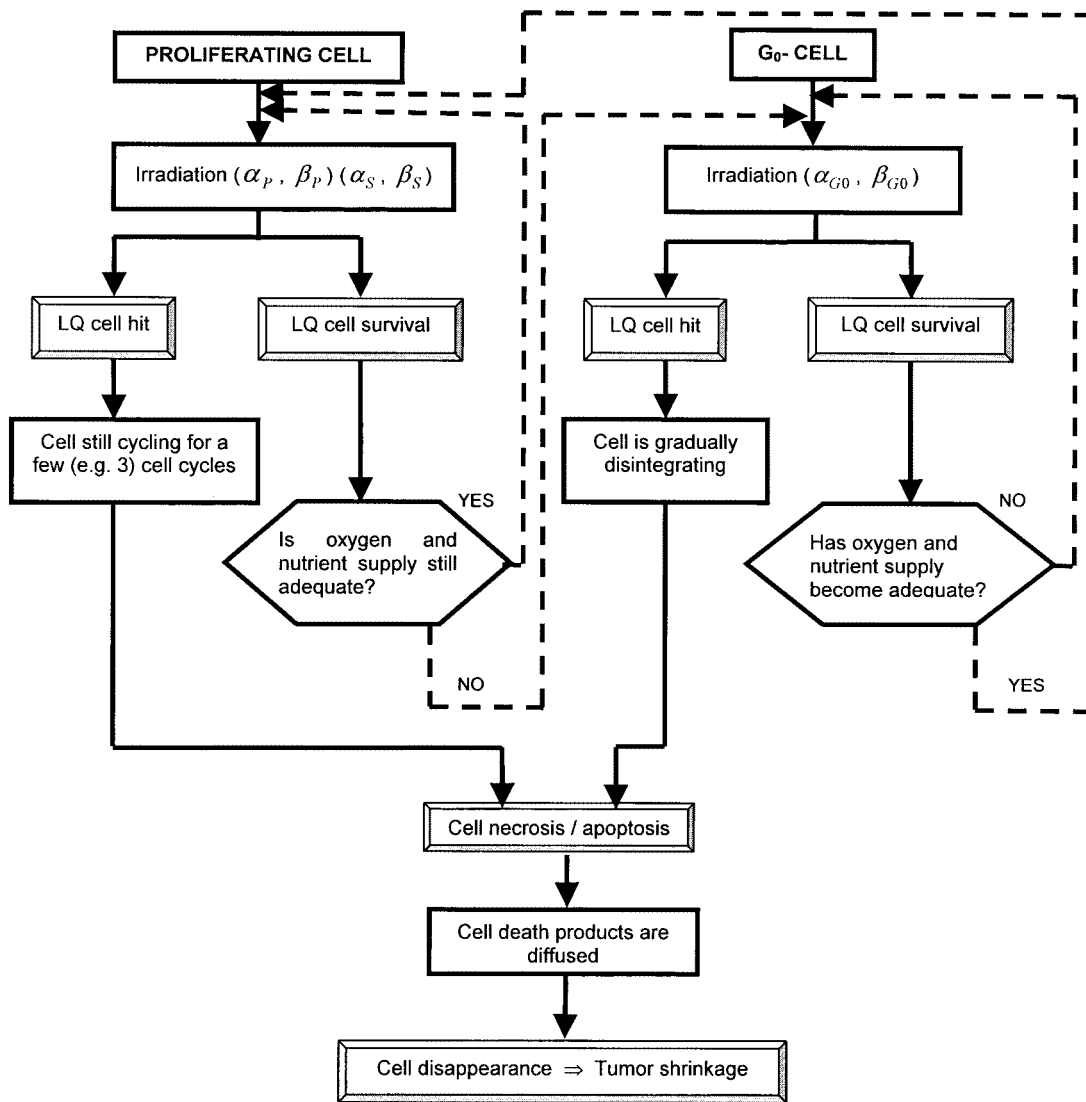
Fig. 2. Simplified flowchart for the response of a single tumor cell to irradiation. Symbol explanation: α_P and β_P stand for the α and β parameters of the LQ model for the tumor proliferating cells excluding those in phase S. The subscript S denotes cells in the DNA synthesis phase, whereas the subscript G_0 denotes cells in the resting (dormant) phase G_0.

and β parameters of the linear-quadratic (LQ) model are assumed: one set for the proliferating cell cycle phases except the S phase, a second one for the S phase, and a third one for the resting G_0 phase. The reason for this is the experimentally established different values of radiosensitivity in the previously mentioned phases. The radiobiological parameters of the tumor cells (α and β parameters of the LQ model) are obtained by fitting the LQ model to an experimental survival curve. However these values are often not very accurate, as a "tradeoff" between α and β allows a range of combinations of the two parameters to fit the data almost equally well. A useful alternative for the calculation of the linear component of cell killing is to use low-dose-rate irradiation. The cell survival curve at a low dose rate seems to extrapolate the initial slope of the high-dose-rate curve [3].

2) The response of each cell to irradiation leading to absorbed dose D is described by the LQ model. According

to this model, the survival probability S of the cell is given by the expression

$$S = \exp\left[-\left(\alpha D + \beta D^2\right)\right] \qquad (1)$$

where α and β are the above-mentioned parameters [3], [4]. It is noted that (1) is effective after the expiration of a time interval sufficient for the sublethal damage to be repaired. The flowchart of Fig. 2 is employed.

C. Tumor Expansion and Shrinkage

1) A 3-D mesh quantizing the volume occupied by the cell culture is used. This volume includes the tumor as well as part of the enclosing nutrient medium. Each geometrical cell of the mesh can be occupied by a single tumor cell, nutrient medium or products of cell death (either necrotic or apoptotic).

2) The total space occupied by the simulated cell culture has been currently confined by our group to $100 \times 100 \times 100$
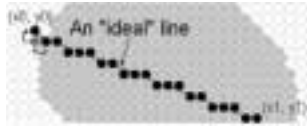
Fig. 3. A line-drawing algorithm (shown for simplicity in two dimensions) is applied to construct the best possible approximation of an ideal line given a discretizing mesh. The white geometrical cells are occupied by a nutrient medium while the gray ones represent tumor cells.

Fig. 4. In the case of tumor expansion, the cell at $(x0, y0)$ in Fig. 3 will not be connected with the rest of the tumor if it shifts diagonally. Therefore, the diagonal shift is replaced by two orthogonal shifts.

mesh cells. This limit depends on the available computer memory and power as well as on the maximum tolerable runtime.

3) Horizontal, vertical, and diagonal communication between cells is possible.

4) The tumor spheroid formation starts with the placement of a single tumor cell at the stage of mitosis at the center of the mesh. A tumor cell can divide even if there is no free space for the daughter cell to be accommodated.

5) The cell lysis and apoptosis products are gradually diffused toward the outer environment of the tumor. In case of *in vivo* tumor growth, such substances are expected to be partly ingested by phagocytes. In this case, the macroscopic result of this mechanism is tumor shrinkage due to the exertion of external pressures.

6) Tumor expansion is computationally achieved by shifting a cell chain from the newly occupied mesh cell toward the external environment of the tumor in a random direction. The shifting direction is defined using two random numbers that denote the azimuthal angle and the polar angle in spherical coordinates. A simple line drawing algorithm is used (Fig. 3). The following additional rule has been introduced in order to preserve tumor connectivity. A cell is considered to be connected with the tumor spheroid if there exists another cell in the tumor spheroid in a unit distance (equal to the length of the edge of a geometrical cell) from it. Diagonal shifts induce displacements equal to ($\sqrt{2}\times$ unit distance) or ($\sqrt{3}\times$ unit distance) and are therefore omitted for cells lying on the external layer of the tumor spheroid (Figs. 3 and 4).

7) In a similar way, tumor shrinkage is computationally achieved by shifting a cell chain from the external environment of the tumor toward the cell that has to disappear in a random direction (Fig. 3). Tumor shrinkage does not appear to considerably affect the tumor connectivity as was previously defined. Therefore, the additional rule has been omitted in the simulation of tumor shrinkage.

D. Time Quantization and Statistical Behavior of the Phase Durations

1) Time is quantized and measured in appropriate units. In all applications, 1 h has been adopted as the unit of time.

2) The durations of the cell cycle phases follow normal (Gaussian) distribution.

3) The simulation can be considered a row-to-row computation of the cell algorithm for each individual cell. At each time step, the remaining time in the current phase of the cell under examination is reduced by one time unit. The configuration obtained in this way serves as the initial step of the subsequent calculation step.

E. Visualization

Software from Advanced Visual Systems has been used to offer a suite of sophisticated 3-D solutions for facilitating the analysis and the representation of tumor growth modeling results. AVS/Express is a comprehensive software development platform that offers highly interactive 3-D data visualization. It provides utilities for medical data acquisition, volume and surface rendering of human body regions of interest and 3-D data manipulation functionalities like the intersection of data in different cutting planes and orientations. AVS Express enables users to acquire input data sets from the output of tumor growth simulation software and create 3-D models of the patient's anatomy (in the *in vivo* case) and of the tumor cells geometry. The AVS/Express-based application allows the user to simulate the placement and the superposition of the different cell states and combine them into a single 3-D representation. The visualized volumes of three cell states (proliferating, dormant, and necrotic/apoptotic) are combined into a single 3-D scene, since the use of coloring and transparency enables the visualization of complex cell topologies. The final representation obtained can be exported from the package in VRML 1.0 or 2.0 format and become available for study in a machine-independent and interoperable way for local or remote examination through a local network or the Internet.

F. The Case of a Glioblastoma Tumor Spheroid in Vitro

1) Input Parameters: To test the simulation model of tumor growth, the case of a brain tumor spheroid *in vitro* has been considered. Brain tumors, such as glioblastoma multiforme, are highly malignant tumors [4]. Typical mean values and standard deviations of the various phases of the constituting cells are shown in Table 1 [69], [43]. Table 2 [69], [81] shows typical mean values of the α and β parameters of the radiobiological LQ model for the following three cell cycle phase groups: the proliferating phases except the DNA synthesis, i.e., the G_1, G_2 and M phases (α_P, β_P), the DNA synthesis phase, or S phase (α_S, β_S), and the resting G_0 phase (α_{G0}, β_{G0}). The α and β values for the last two groups have been assumed as perturbations of the first group values according to the findings of experimental radiobiology. According to [3], cells in the S-phase tend to be the most radioresistant. Classical experiments that have greatly supported this finding are those performed by

Table 1
Mean Values and Standard Deviations of the Cell Cycle Phase Durations for Brain Tumor Cells

Cell phase	Necrosis (N)	G_0	G_1	DNA Synthesis (S)	G2	Mitosis (M)
Mean Duration	$T_{NM}=40h$	$T_{G0M}=25h$	$T_{G1M}=11h$	$T_{SM}=13h$	$T_{G2M}=4h$	$T_{MM}=2h$
Standard Deviation	$T_{ND}=2h$	$T_{G0D}=5h$	$T_{G1D}=1h$	$T_{SD}=2h$	$T_{G2D}=1h$	$T_{MD}=0h$

Table 2
Mean Values of the LQ Model Parameters for Brain Tumor Cells

| $\alpha_P = 0.6$ Gy^{-1}	$\alpha_S = 0.4$ Gy^{-1}	$\alpha_{G0} = 0.2$ Gy^{-1}
$\beta_P = 0.06$ Gy^{-2}	$\beta_S = 0.04$ Gy^{-2}	$\beta_{G0} = 0.02$ Gy^{-2}

TIME = 1h   TIME = 400h   TIME = 600h
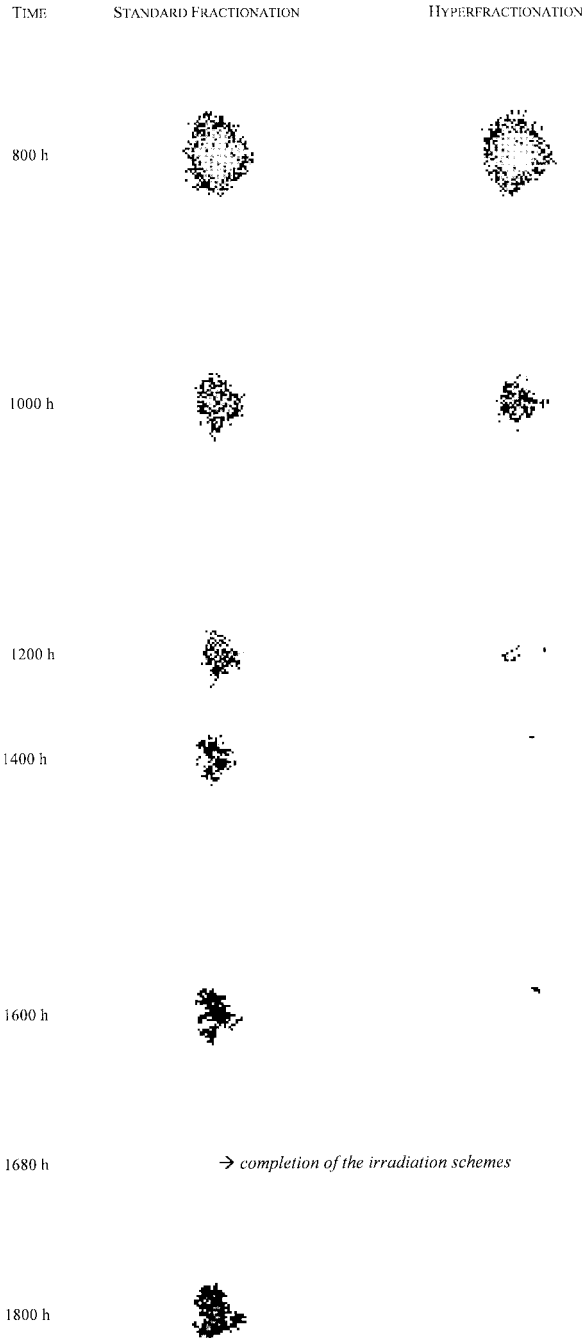
Fig. 5. Simulated evolution of a brain tumor spheroid *in vitro* (equatorial cross section). Gray scale code: white: nutrient medium; light gray: dead cells; dark gray: cells in G_0; black: cells in proliferating phases.

Fig. 6 column headers: TIME — STANDARD FRACTIONATION — HYPERFRACTIONATION

800 h

1000 h

1200 h

1400 h

1600 h

1680 h → *completion of the irradiation schemes*

1800 h

Sinclair and Morton [44]. The survival curves showed that it was mainly the *shoulder* of the curve that changed in the various cell cycle phases. The shoulder was greatest for cells in S. Therefore, the initial slope (which equals the value of the α parameter of the LQ model) is minimum for the S phase compared with the rest of the cell cycle phases. This is the reason why a value for α_S smaller than the average value for α_P has been assumed. Furthermore, as hypoxic cells in G_0 are even more radioresistant, an even smaller value for α_{G0} has been chosen [3]. As the β behavior has not been equally well established, smaller values for β_S and β_{G0} have been chosen also (thus further contributing to an increase in the surviving fraction).

The mean time required for the disappearance of the cell death products from the tumor spheroid has been assumed to be 10 h. Although this time interval seems to be rather small, it was selected in order to quickly demonstrate the ability of the model to simulate tumor shrinkage. More realistic values are expected to arise during experimental tests.
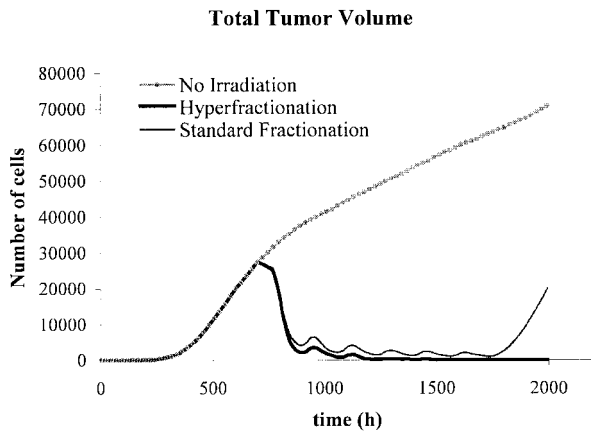
2) Simulation of Fractionated Radiotherapeutic Schemes: The standard and the hyperfractionation schemes (2 Gy once a day, 5 days a week, 60 Gy in total, and 1.2 Gy twice a day, 5 days per week, 72 Gy in total, respectively) have been simulated. Irradiation begins 672 h after the placement of a single tumor cell in the phase of mitosis at the center of the discretizing mesh. Figs. 5 and 6 show an equatorial section of the initially developing and subsequently responding to irradiation tumor. The various classes of cell phases (proliferating cells, cells in the G_0 phase, cells in necrosis/apoptosis) can be readily distinguished. It is evident that repopulation during radiotherapy is kept substantially lower by hyperfractionation

Fig. 6. Simulated response of the tumor of Fig. 5 to the (left) standard fractionation scheme (2 Gy once a day, 5 days per week, 60 Gy in total) and (right) hyperfractionation scheme (1.2 Gy twice a day, 5 days per week, 72 Gy in total). The gray scale code and the time reference of Fig. 5 is used. Irradiation begins 672 h after the placement of a single tumor cell in the phase of mitosis at the center of the discretizing mesh.
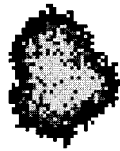
TIME = 2000 h

Fig. 7. Regrowth of the brain tumor after completion of the standard fractionation scheme.

Fig. 8. Total volume (number of living and dead cells) of a brain tumor spheroid as a function of time without external interventions and by applying the standard fractionation (2 Gy once a day, 5 days per week, 60 Gy in total) and the hyperfractionation scheme (1.2 Gy twice a day, 5 days per week, 72 Gy in total) respectively. Irradiation begins 672 h after the placement of a single tumor cell in the phase of mitosis at the center of the discretizing mesh.

than by standard fractionation. This is in accordance with extensive experimental findings [3]. Fig. 7 depicts the eventual regrowth of the tumor from its foci, which survived standard fractionation radiotherapy. Fig. 8 shows the total volume of a brain tumor spheroid as a function of time without external interventions and by applying the standard fractionation and the hyperfractionation schemes, respectively. Good qualitative agreement with the experimentally expected behavior has been noticed in all cases. In the two curves concerning the irradiated tumor, the repopulation effect of the weekend pause can be easily distinguished.

Fig. 9 has been produced using the visualization package AVS/Express 4.2. and depicts a 3-D representation of the external surface of the tumor spheroid under consideration. Both snapshots correspond to the instant $t = 800$ h after the placement of a single tumor cell in the phase of mitosis at the center of the discretizing mesh. The left panel corresponds to the case where no external interventions are applied. The right panel corresponds to the case where the hyperfractionation scheme (1.2 Gy twice a day, 5 days per week, 72 Gy in total) has been applied starting at $t = 672$ h. Cell death is apparently much more pronounced on the right panel as expected. The dissecting planes illustrate how the equatorial cross sections to which Fig. 5–7 correspond have been obtained.
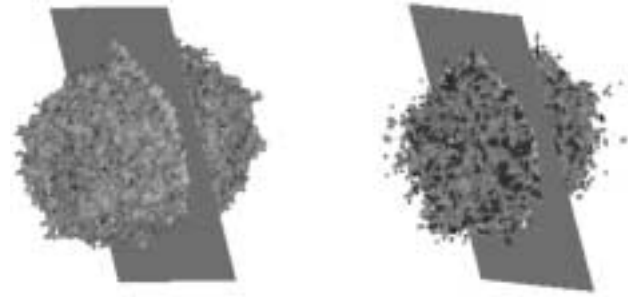
Fig. 9. A 3-D representation of the external surface of a brain tumor spheroid using AVS/Express 4.2. The snapshots correspond to the instant $t = 800$ h. Left: no external interventions take place. Right: the hyperfractionation scheme (1.2 Gy twice a day, 5 days per week, 72 Gy total) is applied starting at $t = 672$ h. Gray scale code: white: nutrient medium; black: products of cell necrosis/apoptosis; light gray: cells in G_0; dark gray: cells in proliferating phases. The dissecting plane illustrates the equatorial cross sections to which Figs. 5–7 correspond.

A typical simulation run of 12 weeks for $100 \times 100 \times 100$ geometrical cells lasts about 7 min on an AMD Athlon XP 1800 machine (786MB RAM). The Visual Fortran 6.0 programming language has been used.

3) Computational Stability Issues: Appropriate pseudorandom number generators are used in order to simulate the statistical character of specific phenomena during the cell proliferation and irradiation. However, if a simulation of tumor growth and response to irradiation begins with a single tumor cell placed at the center of the nutrient medium with different random number generator seeds and/or different ways of scanning of the discretizing mesh, the standard deviation of the total tumor volume could be as high as 60% of the mean value obtained with different executions at a given instant. In order to "stabilize" the predictions, we tried to start simulation of the tumor spheroid formation and behavior with the placement of a small multicellular spheroid with varying number of cells. By starting the simulation procedure with a multicellular spheroid of 5000 cells, we observed that the standard deviation of the total tumor volume decreased to as low as 4% rendering therefore the predictions more reliable.

G. Discussion

The simulation model presented (consisting of a biophysical and a visualization part) provides a novel platform for both gaining insight into the biological mechanisms involved in tumor *growth in vitro* or during the early avascular stages of *in vivo* tumor growth. Optimization of dose fractionation during radiation therapy by performing "*in silico*" experiments is also a practical target. Therefore, the performance of expensive (in terms of both time and money) *in vitro* experiments might be substantially reduced. Although at this stage only a qualitative agreement of the system predictions with the experimental observations has been confirmed, it is expected that a more detailed description of the various biophysical mechanisms involved (e.g., diffusion of oxygen and glucose, the effect of the genetic profile of the tumor such as the status of the p53 gene on the irradiation response, etc.) can add a more clinically significant dimension to the simulation output.

As the simulation model is quite general, the cytokinetic and radiobiological properties of any particular type of tumor cells (able to form tumor spheroids in culture) can be the input to the computer program implementing the analysis presented. Therefore, apart from the provision of the cytokinetic and radiobiological data (α and β values of the linear quadratic model) for the specific tumor cells, no modifications to the code are in principle necessary. Obviously, experimental feedback should always be used in order to improve the reliability of the model.

## IV. In Vivo Tumor Growth and Response to Radiation Therapy: An In Silico Model

The assumptions and the treatment that follow pertain to the *in vivo* simulation model developed by our research group [42], [73].

A. Data Acquisition and Three Dimensional Visualization

As a first step, the imaging data (e.g., CT, MRI, PET slices, possibly fused), including the definition of the tumor contour and the anatomical structures of interest, the histopathologic (e.g., type of tumor) and the genetic data (e.g., p53 status, if available) of the patient are appropriately collected. The output of the above procedure is introduced into the 3-D visualization package AVS-Express, which performs the visualization of both the tumor and the surrounding region of interest by combining volume and surface rendering techniques. In the case of radiotherapy, the distribution of the absorbed dose (e.g., in Gy) in the region of interest at the end of the physical treatment planning procedure is also acquired.

B. Biological Activity of a Solid Tumor in Vivo

The description of the biological activity of the tumor [1]–[4], [8], [14], [82] is implemented by introducing the notion of the "geometrical cell." A 3-D discretizing mesh is superimposed on the anatomical region of interest (Fig. 10). Each geometrical cell of the mesh belonging to the tumor contains a number of biological cells "residing" in various phases within or out of the cell cycle ($G1, S, G2$, Mitosis, G_0, Necrosis). Within each geometrical cell, a number of classes of biological cells (compartments), each one characterized by the phase in which its cells are found (within or out of the cell cycle), are defined. Sufficient registers are used in order to characterize the state of each geometrical cell and each phase class within it (e.g., the number of biological cells in phase $G1$, the time spent in phase $G1$). The number of biological cells constituting each phase class is initially estimated according to the position of the geometrical cell within the tumor, the metabolic activity in the local area (e.g., based on PET, functional MRI). In particular, the relative distribution of the biological cells within each one of the proliferating phases ($G1, S, G2$, or M) is estimated using the mean duration of each cell cycle phase of the specific tumor. The simplified cytokinetic model of Fig. 1 is considered. Both necrotic and apoptotic cell death are taken into account. The mechanical properties of the surrounding tissue are also taken into account in a rather primitive way (e.g., absolute lack of deformability in the bone).
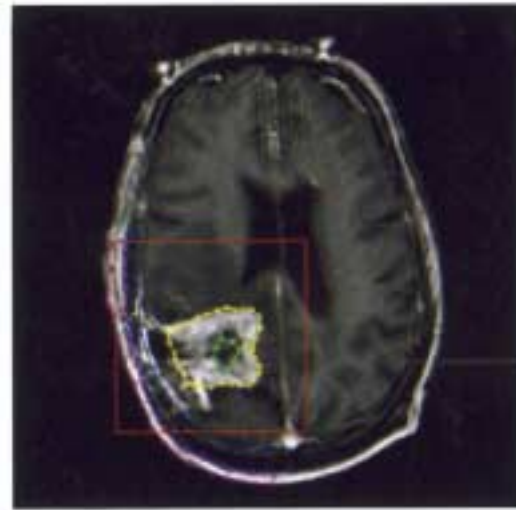

Fig. 10. An MRI slice depicting a grade-IV astrocytoma recently irradiated. Both the clinical volume of the tumor and its central necrotic area have been delineated. The present case has been considered for the preliminary checks of the simulation model.

A simplifying assumption dictates that each geometrical cell of the mesh can "normally" accommodate a constant number of biological cells (NBC). In case that the actual number of alive and dead (but still morphologically existing) tumor cells contained within a given geometrical cell is reduced to less than NBC/2, then a procedure which attempts to "unload" the remaining biological cells in the neighboring geometrical cells takes place, at the end of which if the geometrical cell becomes empty, is assumed to disappear from the tumor. An appropriate shift of the surrounding geometrical cells leads to a differential tumor shrinkage. This can happen, e.g., after irradiation of a radiation responsive tumor. On the other hand, if the number of alive and dead cells within a given geometrical cell exceeds NBC+NBC/2, then a new adjacent geometrical cell emerges. Its position relative to the "mother" geometrical cell is determined using a random number generator. An appropriate shifting of the surrounding geometrical cells takes place leading to a differential expansion of the tumor. The "newborn" geometrical cell initially contains the excess number of biological cells, which are distributed in the various phase classes proportionally to the distribution in the "mother" geometrical cell just before the emergence of the newborn geometrical cell. Apparently, the geometrical cell size depends on the volume of the tumor and the computational resources available and determines the quantization error of the model.

The geometrical mesh covering the anatomic area of interest is scanned every T units of time. For each phase class of a given geometrical cell, behavior algorithms based on the cell cycle phase duration of the tumor cells, the distance from the external boundary of the tumor, the LQ model, the genetic data of the tumor (e.g., wild or mutated p53, bcl-2 genes), determine the updated state. Again, for simplification purposes, all biological cells constituting each phase class within the same geometrical cell are assumed to be synchronized. Biological cells belonging to the same phase class of different
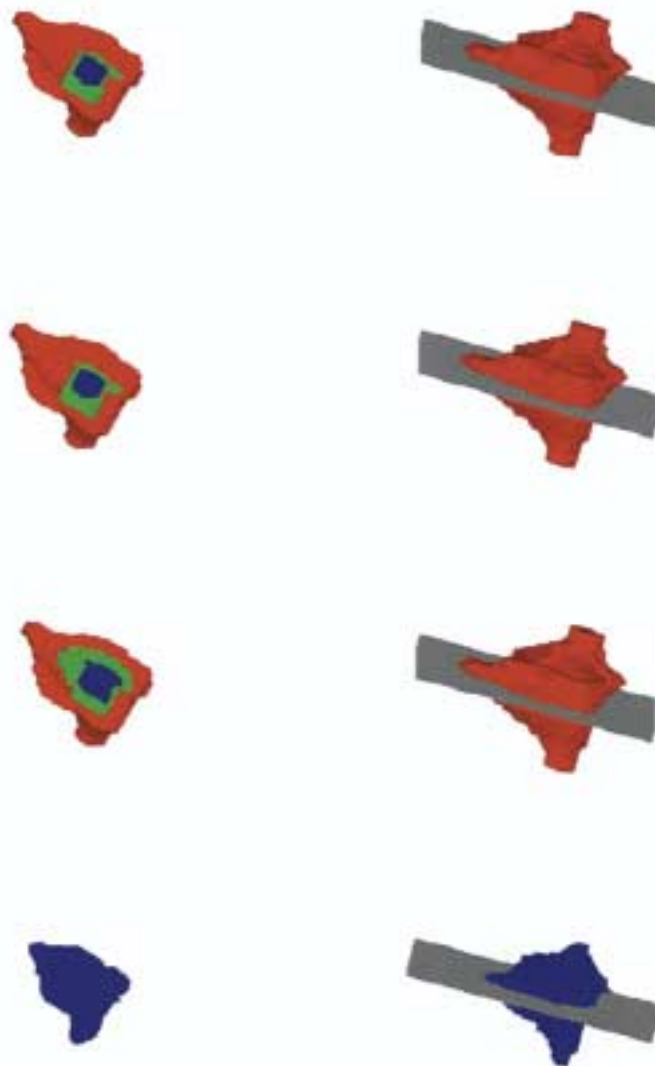
Fig. 11. Irradiation according to the standard fractionation scheme (2 Gy once a day, 5 days per week, 60 Gy in total). Left panel: 3-D sections of the tumor shown in the right panel. Top row: before the beginning of irradiation. Second row: one fictitious day after the beginning of irradiation. Third row: two fictitious days after the beginning of irradiation. Bottom row: three fictitious days after the beginning of irradiation. Color code red: proliferating cell layer; green: dormant cell layer (G_0); blue: dead cell layer. The coloring criterion "99.8%" used to visualize the predictions has been defined as follows. "For a geometrical cell of the discretizing mesh, if the percentage of dead cells is lower than 99.8% then { if percentage of proliferating cells > percentage of G_0 cells, then paint the geometrical cell red (proliferating cell layer), else paint the geometrical cell green (G_0 cell layer)} else paint the geometrical cell blue (dead cell layer)." The values of certain parameters (e.g., cell loss) have been deliberately exaggerated in order to facilitate the demonstration of the ability of the model to simulate the shrinkage effect.

geometrical cells are generally not synchronized. Random number generators are used in order to simulate the statistical nature of various phenomena.

According to the previously described process, the three dimensional progress of a tumor is simulated. In case that radiotherapy treatment has been prescribed, the distribution of the absorbed dose (e.g., in Gy) in the region of interest is also provided. This distribution is used by the biological simulation software described previously in order to "predict" the most likely spatio–temporal response of the tumor. The visualization procedure described in the beginning of this abstract is followed here too.

C. Preliminary Testing of the Simulation Model: The Case of Grade IV Astrocytoma in Vivo

In order to provide a preliminary check of the algorithms described so far, the following testing procedure has been devised and implemented. A case of grade-IV astrocytoma, recently irradiated, has been selected. A specialist doctor has delineated the clinical boundary of the tumor and its necrotic area based on the corresponding MRI and PET data three months after completion of the irradiation course, when tumor repopulation has occurred (Fig. 10). A cube defining the anatomical region of interest has been superimposed on the imaging slices. The dimensions of each geometrical cell

are 1 mm × 1 mm × 1 mm. Such a volume contains roughly 10^6 biological cells (NBC $= 10^6$).

As no information about the metabolic activity (and therefore the density of the tumor neovasculature) prior to irradiation was available (e.g., through PET or functional MRI) for the particular case considered, the only growth support criterion applied so far was the minimization of the distance from the outer surface of the tumor. This implies that biological cells residing in the outer layer of the tumor can be adequately oxygenated and fed whereas the inner part of the tumor lacks efficient neovasculature and therefore oxygenation and nourishment. Obviously, this may not be the case in a large number of tumors. If, e.g., the metabolic imaging data (e.g., PET, SPECT, functional MRI) prior to irradiation suggest that the metabolic activity of the tumor is rather uniform throughout its volume, the growth support criterion would become rather uniform as well. Therefore, the previously predicted layered repopulation structure of the tumor would be replaced by a more uniform one.

The standard fractionation scheme (2 Gy once a day, 5 days per week, 60 Gy total) has been simulated. The LQ model parameters of the tumor are: $\alpha = 0.6$ Gy^{-1}, $\beta = 0.06$ Gy^{-2} [81, radiosensitive tumor] and are assumed to remain constant through the different cell cycle phases. Cells hit by the irradiation are assumed to carry out two mitoses before entering the necrotic phase. For the visualization purposes during this time interval (3/2 of the cell cycle duration) the cells destined to die are considered to have already been dead.

For the specific type of tumor, all nonclonogenic cells are considered to be necrotic (sterile cells are not taken into account). A typical clonogenic cell density is 10^7 cells/cm^3 ($=10^4$ cells/mm^3) [68]. We assume a clonogenic cell density of 2×10^4 cells/mm^3 in the proliferating cell layer (a 6-mm-thick layer from the outer boundary of the tumor), 10^4 cells/mm^3 in the G_0 cell layer (a 1-mm-thick layer surrounding the central necrotic region) and 0.2×10^4 cells/mm^3 in the dead cell layer of the tumor. Within each geometrical cell the initial distribution of the clonogenic cells through the cell cycle phases depends on the layer of the tumor in which the geometrical cell belongs. More precisely, in the proliferating cell layer 70% of the clonogenic cells are assumed to be in the cycling phases and 30% in the G_0 phase. In the G_0 cell layer 30% of the clonogenic cells are in the cycling phases and 70% in the G_0 phase. Finally, in the dead cell layer, 10% of the clonogenic cells are in the cycling phases and 90% in the G_0 phase.

Other parameters of importance include the growth fraction of the tumor (initially taken to be 40% [3, p. 15]), the cell cycle duration $T_C = 30$ h, the cell cycle phase durations $T_{G1} = 11$ h, $T_S = 13$ h, $T_{G2} = 4$ h, $T_M = 2$ h, $T_{G0} = 25$ h [69], and the cell loss factor taken to be equal to 0.9 [3, p. 15]. Certainly such a high loss factor is unrealistic in the case of astrocytoma that has been considered. It has nevertheless been used in order to facilitate the demonstration of the ability of the model to simulate the shrinkage effect. We assume that the total cell loss factor is the sum of the cell loss factor due to necrosis (0.8) and the cell loss


(a)

(b)

(c)

(d)
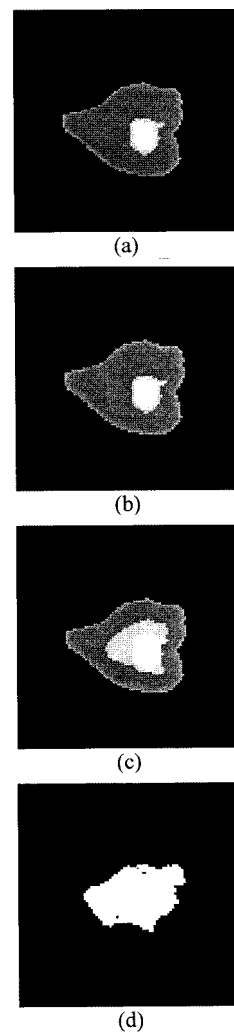
Fig. 12. (a) A centrally located slice of the tumor before the beginning of irradiation. The dark gray geometrical cells near the outer boundary of the tumor constitute the proliferating cell layer. The light gray and white geometrical cells constitute the $G0$ cell layer and the dead cell layer of the tumor respectively. The "99.8%" coloring criterion introduced in Fig. 11 is applied with the following modifications. Red has been substituted by dark gray, green by light gray and blue by white. (b) Simulated response of the tumor to radiation therapy one fictitious day after the beginning of the radiotherapy course. (c) Simulated response of the tumor to radiation therapy two fictitious days after the beginning of the radiotherapy course. (d) Simulated response of the tumor to radiation therapy three fictitious days after the beginning of the radiotherapy course. The values of certain parameters (e.g., cell loss) have been deliberately exaggerated in order to emphasize the ability of the model to simulate tumor shrinking as a response to radiation therapy.

factor due to apoptosis (0.1). The probabilities of cell loss per hour due to necrosis (0.01) and due to apoptosis (0.0013) are derived from the above-mentioned value of the cell loss factor according to [3, p. 15]. Furthermore, in contrast with the *in vitro* model in the present version of the *in vivo* model, no variation in the α and β LQ parameters has been considered. Obviously such a variation can be easily incorporated in the computer code.

The computer code has been developed in Microsoft Visual C++ 6 and Microsoft Visual Basic 6. As far as the computational demands are concerned, an execution of the radi-
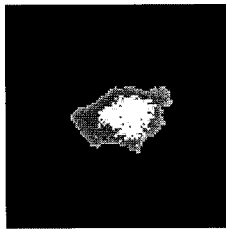
Fig. 13. Visualization of the tumor status on the third fictitious day after the beginning of the radiotherapy course where a coloring criterion of "99.95%" instead of "99.8%" has been applied.

(a)

(b)

(c)

(d)
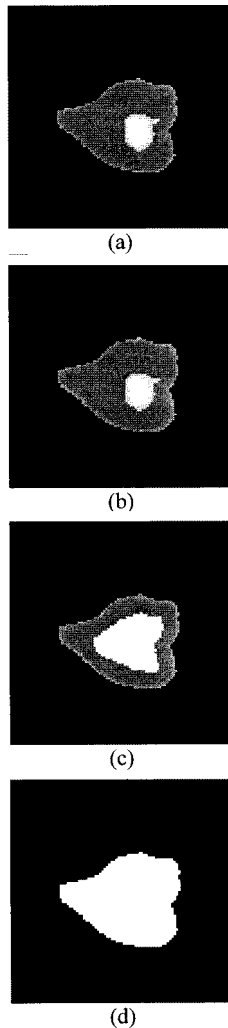
Fig. 14. Simulation results using a reduced value for the cell loss factor (0.5). Standard dose fractionation is considered. A centrally located slice of the tumor (a) before the beginning of the radiotherapy course and (b) one, (c) two, and (d) three fictitious days after the beginning of the radiotherapy course. Due to a reduced cell loss factor, there is no observable shrinkage of the tumor. This seems to be a more clinically compatible scenario in the case of astrocytoma.

ation therapy simulation of 6 weeks (96 × 96 × 96 geometrical cells, each one of dimensions 1 mm × 1 mm × 1 mm) on an AMD Athlon XP 1800 machine (786 MB RAM) takes about 10 min.

The testing predictions depicted in Figs. 11–14 demonstrate the ability of the model to adequately simulate cell death and tumor shrinkage. In order to emphasize this poten-

tial of the model, the values of certain parameters (e.g., cell loss) have been deliberately exaggerated. Systematic comparison with clinical data that is currently under way is expected to lead to more clinically relevant parameter values. Details on the simulation sequences and the visualization criteria are to be found on the respective figure captions.

D. Discussion

The previously described *in vivo* paradigm deals with a novel approach to the modeling of a clinically manifested solid tumor. The simulation model is capable of satisfactorily simulating characteristics of tumor behavior such as tumor repopulation, expansion and shrinkage. The software system developed is currently undergoing an extensive validation and optimization procedure based on pertinent clinical and laboratory data concerning, e.g., astrocytoma irradiation. Nevertheless, it should be stressed that all versions of the simulation model will always have a statistical/probabilistic nature, as cancer itself is a highly complex and partly unpredictable disease.

V. CONCLUSION

The concept of *in silico* radiation oncology has been clarified by means of a brief review of the literature concerning experimental, mathematical, 3-D computer simulation *models* of tumor growth and response to radiation therapy as well as by two simulation and visualization paradigms developed by our research group.

The first paradigm refers to *in vitro* tumor spheroid development and irradiation whereas the second one refers to *in vivo* clinical tumors treated by fractionated radiation therapy. The basic elementary phenomena taking place during the tumor growth and response processes have been pointed out. The salient simulated phenomena include: cell metabolism, cell division and interaction, cell response to irradiation and tumor expansion and shrinkage. In the case of the *in vivo* simulation model, adequate algorithms describing the acquisition and preprocessing of clinical data have been proposed and implemented. Specific applications of the models to experimental and clinical cases have been described and the behavior of the model is two- and three-dimensionally visualized.

Good qualitative agreement with experimental and clinical observations strengthens the applicability of the models to real situations. Concerning the *in vitro* case, the predictions compare fairly well with those of Duechting *et al.* [69], [76] who addressed the most similar problem to the one treated by our group, although the formulation of the irradiation response algorithms is substantially different. Regarding the *in vivo* case as the specific problem treated by the authors (fractionated irradiation of a large *in vivo* tumor based on actual imaging data) seems not to have been dealt with by other researchers, no comparison with other models has been made. Further systematic testing and adaptation of the model is under way. This procedure basically consists of comparisons of the model predictions with experimental and clinical

data before, during and after the radiotherapy course. Eventual discrepancies will lead to better estimation of certain model parameters such as the alpha and beta values of the LQ model. Inclusion of the effect of other treatment modalities such as chemotherapy or gene therapy as well as the response of the adjacent normal tissues to irradiation and other modalities is under investigation. The fact that both simulation models have a clear modular character is expected to substantially facilitate the clinical adjustment and extension procedures.

Therefore, an integrated and patient individualized decision support and spatio–temporal treatment planning system is expected to emerge after the completion of the necessary experimental and clinical trials. Such a system is expected to substantially contribute to the advancement of basic cancer research leading to the further clarification of the mechanisms responsible for tumor growth and response to various treatments. Furthermore, it could serve as a basis for "educating" the patient by means of imaging demonstrations on the likely natural development and treatment responsiveness of the cancer so that he/she can positively contribute to the discussion on the treatment procedure.

REFERENCES

[1] H. Lodish, D. Baltimore, A. Berk, S. Zipursky, P. Matsudaira, and J. Darnell, *Molecular Cell Biology*. New York, NY: Scientific , 1995, pp. 1247–1294.

[2] J. Watson, N. Hopkins, J. Roberts, J. Steitz, and A. Weiner, *Molecular Biology of the Gene*, 4th ed. Menlo Park, CA: The Benjamin/Cummings, 1987, pp. 1006–1096.

[3] G. Steel, Ed., *Basic Clinical Radiobiology*. London, UK: Arnold, 1997, pp. 15, 47–48, 52–57, 123–131, 153, 161.

[4] C. Perez and L. Brady, *Principles and Practice of Radiation Oncology*. Philadelphia, PA: Lippincott-Raven, 1998, pp. 784–785.

[5] J. F. Fowler, "Review of radiobiological models for improving cancer treatment," in *Modeling in Clinical Radiobiology*, K. Baier and D. Baltas, Eds. Freiburg, Germany: Albert-Ludwigs-University, 1997, Freiburg Oncology Series, Monograph no. 2, ch. 1, pp. 1–14.

[6] M. Santini, G. Rainaldi, and P. Indovina, "Multicellular tumour spheroids in radiation biology," *Int. J. Radiat. Biol.*, vol. 75, no. 7, pp. 787–799, 1999.

[7] R. Jostes, M. Williams, M. Barcellos-Hoff, T. Hoshino, and D. Deen, "Growth delay in 9L rat brain tumor spheroids after irradiation with single and split doses of X rays," *Radiat. Res.*, vol. 102, no. 2, pp. 182–189, 1985.

[8] J. Casciari, S. Sotirchos, and R. Sutherl, "Variations in tumor cell growth rates and metabolism with oxygen concentration, glucose concentration, and extracellular pH," *J. Cellular Physiol.*, vol. 151, pp. 386–394, 1992.

[9] M. Santini and G. Rainaldi, "Three-dimensional spheroid model in tumor biology," *Pathobiology*, vol. 67, pp. 148–157, 1999.

[10] C. Nirmala, J. S. Rao, A. C. Ruifrock, L. A. Langford, and M. Obeyesekere, "Growth characteristics of glioblastoma spheroids," *Int. J. Oncology*, vol. 19, pp. 1109–1115, 2001.

[11] J. P. Freyer and R. M. Sutherland, "Regulation of growth and development of necrosis in EMT6/Ro multicellular spheroids by the glucose and oxygen supply," *Cancer Res.*, vol. 46, pp. 3504–3512, 1986.

[12] J. A. Adam and S. A. Maggelakis, "Diffusion regulated growth characteristics of a spherical prevascular carcinoma," *Bull. Math. Biol.*, vol. 52, pp. 549–582, 1990.

[13] J. J. Casciari, S. V. Sotirchos, and R. M. Sutherland, "Glucose diffusivity in multicellular tumor spheroids," *Cancer Res.*, vol. 48, pp. 3905–3909, 1988.

[14] W. Duechting, "Krebs, ein instabiler Regelkreis. Versuch einer Systemanalyze," *Kybernetik*, vol. 5, no. 2, pp. 70–77, 1968.

[15] R. A. Gatenby, "Models of tumor–host interaction as competing populations: Implications for tumor biology and treatment," *J. Theor. Biol.*, vol. 176, pp. 447–455, 1995.

[16] R. Uddin and I. M. Saeed, "Structure and growth of tumors: The effect of Cartesian, cylindrical, and spherical geometries," *Ann. New York Acad. Sci.*, vol. 858, pp. 127–136, 1998.

[17] H. P. Greenspan, "On the growth and stability of cell cultures and solid tumors," *J. Theor. Biol.*, vol. 56, pp. 229–242, 1976.

[18] H. Bremermann, "Reliability of proliferation controls. The Hayflick limit and its breakdown in cancer," *J. Theor. Biol.*, vol. 97, pp. 641–662, 1982.

[19] R. Demicheli, R. Foroni, A. Ingrosso, G. Pratesi, C. Sorano, and M. Tortoreto, "An exponential-Gompertzian description of LoVo cell tumor growth from *in vivo* and *in vitro* data," *Cancer Res.*, vol. 49, pp. 6543–6546, 1989.

[20] J. J. Terz, W. Lawrence, Jr., and B. Cox, "Analysis of the cycling and noncycling cell population of human solid tumors," *Cancer*, vol. 40, pp. 1462–1470, 1977.

[21] G. Hejblum, D. Costagliola, A.-J. Valleron, and J.-Y. Mary, "Cell cycle models and mother–daughter correlation," *J. Theor. Biol.*, vol. 131, pp. 255–262, 1988.

[22] K. A. Heichman and J. M. Roberts, "Rules to replicate by," *Cell*, vol. 79, pp. 557–562, 1994.

[23] D. Wiarda and C. C. Travis, "Determinability of model parameters in a two-stage deterministic cancer model," *Math. Biosci.*, vol. 146, pp. 1–13, 1997.

[24] R. A. Gatenby and E. T. Gawlinski, "A reaction–diffusion model of cancer invasion," *Cancer Res.*, vol. 56, pp. 5745–5753, 1996.

[25] K. Iwata, K. Kawasaki, and N. Shigesada, "A dynamical model for the growth and size distribution of multiple metastatic tumors," *J. Theor. Biol.*, vol. 201, pp. 177–186, 2000.

[26] A. D. Murray, "Creative blocks: Cell-cycle checkpoints and feedback controls," *Nature*, vol. 359, pp. 599–604, 1992.

[27] I. I. H. Chen and R. L. Prewitt, "A mathematical representation for vessel network," *J. Theor. Biol.*, vol. 97, pp. 211–219, 1982.

[28] D. Balding and D. L. S. Mc Elwain, "A mathematical model of tumor-induced capillary growth," *J. Theor. Biol.*, vol. 114, pp. 53–73, 1985.

[29] S. Michelson and J. T. Leith, "Possible feedback and angiogenesis in tumor growth control," *Bull. Math. Biol.*, vol. 59, pp. 233–254, 1997.

[30] W. Duechting and T. Vogelsaenger, "Three-dimensional pattern generation applied to spheroidal tumor growth in a nutrient medium," *Int. J. Biomed. Comput.*, vol. 12, no. 5, pp. 377–392, 1981.

[31] W. Duechting, "Tumor growth simulation," *Comput. Graphics*, vol. 14, pp. 505–508, 1990.

[32] G. Stamatakos, N. Uzunoglu, K. Delibasis, M. Makropoulou, N. Mouravliansky, and A. Marsh, "A simplified simulation model and virtual reality visualization of tumor growth *in vitro*," *Future Generation Comput. Syst.*, vol. 14, pp. 79–89, 1998.

[33] G. S. Stamatakos, N. K. Uzunoglu, K. Delibasis, M. Makropoulou, N. Mouravliansky, and A. Marsh, "Coupling parallel computing and the WWW to visualize a simplified simulation of tumor growth *in vitro*," in *Proc. Int. Conf. Parallel and Distributed Processing Techniques and Applications, PDTA'98*, H. R. Arabnia, Ed. Las Vegas, NV, 1998, pp. 526–533.

[34] G. Stamatakos, N. Uzunoglu, K. Delibasis, N. Mouravliansky, M. Makropoulou, and A. Marsh, "Using VRML in a client–server architecture to visualize a simplified simulation model of tumor growth *in vitro*," in *Proc. 20th Annu. Int. Conf.—IEEE/EMBS*, Hong Kong, 1998, pp. 2834–2837.

[35] G. Stamatakos, E. Zacharaki, N. Mouravliansky, K. Delibasis, K. Nikita, N. Uzunoglu, and A. Marsh, "Using Web technologies and meta-computing to visualize a simplified simulation model of tumor growth *in vitro*," in *High-Performance Computing and Networking*. ser. Lecture Notes in Computer Science, P. Sloot, M. Bubak, A. Hoekstra, and B. Hertzberger, Eds. Berlin, Germany: Springer, 1999, vol. 1593, pp. 973–982.

[36] G. Stamatakos, E. Zacharaki, M. Makropoulou, N. Mouravliansky, K. Nikita, and N. Uzunoglu, "Tumour growth *in vitro* and tumour response to irradiation schemes: A simulation model and virtual reality visualization," *Radiother. Oncol.*, vol. 56, Suppl. 1, pp. 179–180, 2000.

[37] G. S. Stamatakos, N. K. Uzunoglu, K. Delibasis, N. Mouravliansky, A. Marsh, and M. Makropoulou, "Tumor growth simulation and visualization: A review and a Web based paradigm," *Studies Health Technol. Informatics*, vol. 79, pp. 255–274, 2000.

[38] T. S. Deisboeck, M. E. Berens, A. R. Kansal, S. Torquato, A. O. Stemmer-Rachmamimov, and E. A. Chiocca, "Pattern of self-organization in tumour systems: Complex growth dynamics in a novel brain tumour spheroid model," *Cell Prolif.*, vol. 34, pp. 115–134, 2001.

[39] R. Wasserman and R. Acharya, "A patient-specific *in vivo* tumor model," *Math. Biosci.*, vol. 136, pp. 111–140, Sept. 1996.

[40] A. R. Kansal, S. Torquato, G. R. Harsh, E. A. Chiocca, and T. S. Deisboeck, "Simulated brain tumor growth dynamics using a three-dimensional cellular automaton," *J. Theor. Biol.*, vol. 203, pp. 367–382, 2000.

[41] A. R. Kansal, S. Torquato, G. R. Harsh, IV, E. A. Chiocca, and T. S. Deisboeck, "Cellular automaton of idealized brain tumor growth dynamics," *BioSystems*, vol. 55, pp. 119–127, 2000.

[42] G. Stamatakos, D. Dionysiou, N. Mouravliansky, K. Nikita, G. Pissakas, P. Georgolopoulou, and N. Uuznoglu, "Algorithmic description of the biological activity of a solid tumour *in vivo*," in *Proc. EUROSIM 2001 Congress*, Delft, The Netherlands, June 26–29, 2001 (CD-ROM Edition).

[43] L. Cohen, *Biophysical Models in Radiation Oncology*. Boca Raton, FL: CRC Press, 1983.

[44] W. Sinclair and R. Morton, "X-ray and ultraviolet sensitivity of synchronized Chinese hamster cells at various stages of the cell cycle," *Biophys. J.*, vol. 5, pp. 1–25, 1965.

[45] C. J. Gillespie, J. D. Chapman, A. P. Reuvers, and D. L. Dugle, "The inactivation of Chinese hamster cells by X rays: Synchronized and exponential cell populations," *Radiat. Res.*, vol. 64, pp. 353–364, 1975.

[46] H. D. Thames, Jr., H. R. Withers, L. J. Peters, and G. H. Fletcher, "Changes in early and late radiation responses with altered dose fractionation: implications for dose—Survival relationships," *Int. J. Radiation Oncology Biol. Phys.*, vol. 8, pp. 219–226, 1982.

[47] R. G. Dale, "The application of the linear-quadratic dose-effect equation to fractionated and protracted radiotherapy," *Br. J. Radiol.*, vol. 58, pp. 515–528, 1985.

[48] H. D. Thames, "An 'incomplete-repair' model for survival after fractionated and continuous irradiations," *Int. J. Radiat. Biol.*, vol. 47, pp. 319–339, 1985.

[49] H. D. Thames, M. E. Rozell, S. L. Tucker, K. K. Ang, D. R. Fisher, and E. L. Travis, "Direct analysis of quantal radiation response data," *Int. J. Radiat. Oncol. Biol. Phys.*, vol. 49, pp. 999–1009, 1986.

[50] J. Denekamp, "Cell kinetics and radiation biology," *Int. J. Radiat. Biol.*, vol. 49, pp. 357–380, 1986.

[51] R. Dale, "The application of the linear-quadratic model to fractionated radiotherapy when there is incomplete normal tissue recovery between fractions, and possible implications for treatments involving multiple fractions per day," *Br. J. Radiol.*, vol. 59, pp. 919–927, 1986.

[52] E. L. Travis and S. L. Tucker, "Isoeffect models and fractionated radiation therapy," *Int. J. Radiation Oncology Biol. Phys.*, vol. 13, pp. 283–287, 1987.

[53] J. F. Fowler, "The linear-quadratic formula and progress in fractionated radiotherapy," *Br. J. Radiol.*, vol. 62, pp. 679–694, 1989.

[54] L. E. Dillehay, "A model of cell killing by low-dose-rate radiation including repair of sublethal damage, $G2$ block, and cell division," *Radiat. Res.*, vol. 124, pp. 201–207, 1990.

[55] S. L. Tucker, H. D. Thames, and J. M. G. Taylor, "How well is the probability of tumor cure after fractionated irradiation described by Poisson statistics?," *Radiat. Res.*, vol. 124, pp. 273–282, 1990.

[56] D. J. Brenner, "Track structure, lesion development and cell survival," *Radiat. Res.*, vol. 124, pp. S29–S37, 1990.

[57] H. D. Thames, S. M. Bentzen, I. Turesson, M. Overgaard, and W. Van de Bogaert, "Time-dose factors in radiotherapy: A review of the human data," *Radiother.Oncol.*, vol. 19, pp. 219–235, 1990.

[58] J. Chen, J. Van de Geijn, and T. Goffman, "Extra lethal damage due to residual incompletely repaired sublethal damage in hyperfractionated and continuous radiation treatments," *Med. Phys.*, vol. 18, pp. 488–496, 1991.

[59] H. D. Thames, T. E. Schultheiss, J. H. Hendry, S. L. Tucker, B. M. Dubray, and W. A. Brock, "Can modest escalations of dose be detected as increased tumor control?," *Int. J. Radiat. Oncol. Biol. Phys.*, vol. 22, pp. 241–246, 1992.

[60] M. Zaider and G. N. Minerbo, "A mathematical model for cell cycle progression under continuous low-dose-rate irradiation," *Radiat. Res.*, vol. 133, pp. 20–26, 1993.

[61] H. R. Withers, "Biologic basis of radiation therapy," in *Principles and Practice of Radiation Oncology*, 2nd ed, C. A. Perez and L. W. Brady, Eds. New York: J. P. Lippincott, 1992, pp. 64–96.

[62] B. Jones and R. Dale, "Mathematical models of tumour and normal tissue response," *Acta Oncologica*, vol. 38, pp. 883–893, 1999.

[63] T. E. Wheldon, A. S. Michalowski, and J. Kirk, "The effect of irradiation on function in self-renewing normal tissues with differing proliferative organization," *Br. J. Radiol.*, vol. 55, pp. 759–766, 1982.

[64] D. A. Haas-Kogan, G. Yount, M. Haas, D. Levi, S. S. Kogan, L. Hu, C. Vidair, D. F. Deen, W. C. Dewey, and M. A. Israel, "p53-dependent G_1 arrest and p53 independent apoptosis influence the radiobiologic response of glioblastoma," *Int. J. Radiat. Oncol. Biol. Phys.*, vol. 36, no. 1, pp. 95–103, 1996.

[65] J. C. Panetta, "A mathematical model of periodically pulsed chemotherapy: Tumor recurrence and metastasis in a competitive environment," *Bull. Mat. Biol.*, vol. 58, pp. 425–447, 1996.

[66] D. A. Cameron, W. M. Gregory, A. Bowman, and R. C. F. Leonard, "Mathematical modeling of tumour response in primary breast cancer," *Br. J. Cancer*, vol. 73, pp. 1409–1416, 1996.

[67] T. Ginsberg, "Modellierung und Simulation der Proliferationsregulation und Strahlentherapie normaler und maligner Gewebe," VDI Verlag, Duesseldorf, Fortschritt-Berichte, Reihe 17: Biotechnik, Nr 140, 1996.

[68] A. Nahum and B. Sanchez-Nieto, "Tumour control probability modeling: Basic principles and applications in treatment planning," *Physica Medica*, vol. 17(xvii), suppl. 2, pp. 13–23, 2001.

[69] W. Duechting, W. Ulmer, R. Lehrig, T. Ginsberg, and E. Dedeleit, "Computer simulation and modeling of tumor spheroid growth and their relevance for optimization of fractionated radiotherapy," *Strahlenther. Onkol.*, vol. 168, no. 6, pp. 354–360, 1992.

[70] W. Duechting, T. Ginsberg, and W. Ulmer, "Modeling of radiogenic responses induced by fractionated irradiation in malignant and normal tissue," *Stem Cells*, vol. 13, (Suppl. 1), pp. 301–306, 1995.

[71] G. Stamatakos, E. Zacharaki, M. Makropoulou, N. Mouravliansky, A. Marsh, K. Nikita, and N. Uzunoglu, "Modeling tumor growth and irradiation response *in vitro*—A combination of high-performance computing and web based technologies including VRML visualization," *IEEE Trans. Inform. Technol. Biomed.*, vol. 5, pp. 279–289, Dec. 2001.

[72] G. Stamatakos, E. I. Zacharaki, N. K. Uzunoglu, and K. S. Nikita, "Tumor growth and response to irradiation *in vitro*: A technologically advanced simulation model," *Int. J. Radiat. Oncol. Biol. Phys.*, vol. 51, Supl. 1, pp. 240–241, 2001.

[73] G. Stamatakos, D. Dionysiou, K. Nikita, N. Zamboglou, D. Baltas, G. Pissakas, and N. K. Uzunoglu, "*In vivo* tumor growth and response to radiation therapy: A novel algorithmic description," *Int. J. Radiat. Oncol. Biol. Phys.*, vol. 51, no. 3, Sup. 1, p. 240, 2001.

[74] M. Kocher and H. Treuer, "Reoxygenation of hypoxic cells by tumor shrinkage during irradiation. A computer simulation," *Strahlenther. Onkol.*, vol. 171, pp. 219–230, Apr. 1995.

[75] M. Kocher, H. Treuer, J. Voges, M. Hoevels, V. Sturm, and R. P. Mueller, "Computer simulation of cytotoxic and vascular effects of radiosurgery in solid and necrotic brain metastases," *Radiother. Oncol.*, vol. 54, pp. 149–156, 2000.

[76] W. Duechting, R. Lehring, G. Rademacher, and W. Ulmer, "Computer simulation of clinical irradiation schemes applied to *in vitro* tumor spheroids," *Strahlenther. Onkol.*, vol. 165, pp. 873–878, 1989.

[77] B. Grant, "Virtual Reality gives medicine a powerful new tool," *Biophoton. Int.*, pp. 40–45, Nov./Dec. 1997.

[78] W. Lorensen and H. Cline, "Marching cubes: High resolution 3D surface construction algorithm," *Comput. Graph.*, vol. 21, no. 3, pp. 163–169, 1987.

[79] B. S. Kuszyk, D. R. Ney, and E. K. Fishman, "The current state of the art in three dimensional oncologic imaging: An overview," *Int. J. Radiat. Oncol. Biol. Phys.*, vol. 33, pp. 1029–1039, 1995.

[80] W. Duechting, "Computermodelle zur Optimierung der Strahlentherapie," *Automatisierungstechnik*, vol. 46, no. 11, pp. 546–552.

[81] B. Jones and C. Bleasdale, "Influence of tumour regression and clonogen repopulation on tumour control by brachytherapy," in *Modeling in Clinical Radiobiology*, K. Baier and D. Baltas, Eds. Freiburg, Germany: Albert-Ludwigs-University, 1997, Freiburg Oncology Series, Monograph no. 2, ch. 14, pp. 116–126.

[82] T. Williams and R. Bjerknes, "Stochastic model for abnormal clone spread through epithelial basal layer," *Nature*, vol. 236, pp. 19–21, 1972.

Georgios S. Stamatakos received the Diploma degree in electrical engineering from the National Technical University of Athens (NTUA), Athens, Greece, in 1987, the M.Sc. degree in bioengineering from the University of Strathclyde, Glasgow, U.K., in 1988, and the Ph.D. degree in physics from the NTUA in 1997.

From 1989 to 1990, he was with the Hellenic Army General Staff, Medical Corps Directorate. From 1991 to 1997, he was a Teaching Assistant in the Department of Physics, NTUA. Since 1997, he has been a Researcher at the Institute of Communication and Computer Systems (ICCS), Department of Electrical and Computer Engineering, NTUA, where he is currently a Research Assistant Professor. His research interests include oncological simulations, radiotherapy optimization, bioinformatics, electromagnetic propagation and scattering, nonionizing radiation safety, and biooptics. He has published over 45 papers in international journals, conferences proceedings, and books.

Dr. Stamatakos is a Member of the Technical Chamber of Greece and the European Society for Engineering and Medicine.

Dimitra D. Dionysiou received the Diploma degree in electrical and computer engineering from the National Technical University of Athens (NTUA), Athens, Greece, in 1998. She is currently working toward the Ph.D. degree at the same university.

Her research interests include oncological simulations, biological process modeling, systems analysis and biomedical engineering. She has published five papers in international conference proceedings and journals.

Evangelia I. Zacharaki was born in Panariti-Korinthos, Greece, in 1977. She received the Diploma degree in electrical and computer engineering from the National Technical University of Athens (NTUA), Athens, Greece, in 1999. She is currently working toward the Ph.D. degree at the same university.

Her research interests include biological process simulations, medical image visualization, and image processing. She has published nine papers in international conferences and journals.

Nikolaos A. Mouravliansky (Student Member, IEEE) was born in Athens, Greece, in 1973. He received the Diploma and the Ph.D. degrees in electrical engineering from the National Technical University of Athens (NTUA), Greece, in 1996 and 2000, respectively.

His research interests include image processing, telemedicine and biomedical engineering. He has published over 15 papers in international conferences and journals.

Konstantina S. Nikita (Senior Member, IEEE) received the Diploma in electrical engineering and the Ph.D. degree from the National Technical University of Athens (NTUA), Athens, Greece, in 1986 and 1990, respectively, and the M.D. degree from the University of Athens, Greece, in 1993.

Since 1990, she has been working as a Researcher at the Institute of Communication and Computer Systems, NTUA. In 1996, she joined the Department of Electrical and Computer Engineering, NTUA, where she is currently an Associate Professor. Her current research interests include applied computational electromagnetics, applications of electromagnetic waves in medicine, medical imaging and image processing, and nonlinear optimization algorithms and applications. She has authored or coauthored 40 papers in refereed international journals and chapters in books and 80 papers in international conference proceedings. She has also co-edited the book *Applied Computational Electromagnetics: State of the Art and Future Trends* (New York: Springer, 2000). She has been the technical manager of a number of European and National Research and Development projects in the fields of bioelectromagnetic interactions and biomedical engineering.

Dr. Nikita is a Member of the Technical Chamber of Greece, the Athens Medical Association, and the Hellenic Society of Biomedical Engineering.

Nikolaos K. Uzunoglu (Senior Member, IEEE) was born in Constantinopole in 1951. He received the B.Sc. degree in electrical engineering from the Istanbul Technical University, Turkey, in 1973 and the M.Sc. and Ph.D. degrees from the University of Essex, U.K., in 1974 and 1976, respectively.

He worked for the Hellenic Navy Research and Development Office from 1977 to 1984. In 1984, he was elected Associate Professor and in 1988 Professor in electrical engineering at the National Technical University of Athens (NTUA), Athens, Greece. He has been Director of the Institute of Communication and Computer Science (ICCS), NTUA, during 1991–1999. His research interests include electromagnetic theory, microwaves, fiber optics, biological process simulations, and biomedical engineering. He has published 150 papers in refereed journals.

Dr. Uzunoglu was the recipient of the 1981 International G. Marconi Award in Telecommunications. He is a member of the Academy of Sciences of Armenia.